(This is a sample cover image for this issue. The actual cover is not yet available at this time.)

Journal of Alloys and Compounds 547 (2013) 63–67

Contents lists available at SciVerse ScienceDirect

Journal of Alloys and Compounds

journal homepage: www.elsevier.com/locate/jalcom

Synthesis, structure and optical properties of single-crystalline In_2O_3 nanowires

N.M.A. Hadia [a,*], H.A. Mohamed [a,b]

[a] Physics Department, Faculty of Science, Sohag University, 82524 Sohag, Egypt
[b] King Saud University, Teachers College, Science Department (Physics), 11148 Riyadh, Saudi Arabia

ARTICLE INFO

Article history:
Received 28 May 2012
Received in revised form 27 August 2012
Accepted 29 August 2012
Available online 5 September 2012

Keywords:
Indium oxide
Nanostructures synthesis
Nanowires
Optical parameters
Photoluminescence

ABSTRACT

Indium oxide In_2O_3 nanowires have been recently synthesized revealing interesting properties and used in various applications. In order to reduce as much as possible the influence of undesired dopants and/or impurities on the observed properties, In_2O_3 nanowires have been grown without the use of catalysts, directly from metallic indium by a vapor transport technique and a controlled oxidation with oxygen–argon mixtures. Depending on the growth conditions (temperature, vapor pressure, oxygen concentration, etc.) different results have been achieved and it has been observed that a 'proper' In condensation on the substrates may enhance the nanowires growth. Detailed structural analysis showed that the In_2O_3 nanostructures are single crystalline with a cubic crystal structure. The grown In_2O_3 nanowires were optically characterized in order to evaluate the absorption coefficient, optical band gap, refractive index and extinction coefficient. Room temperature Photoluminescence (PL) spectrum showed broad and intense blue emission at 375 nm.

1. Introduction

Today the interest in the 'nanowire-like' structures is growing up exponentially for many different materials. The peculiar properties showed by one-dimensional (1D) nanostructures stimulated several discussions about their potential applications in various fields and research on the synthesis of these nano-materials.

In the last few years several functional oxides have been successfully synthesized [1,2] by vapor transport/deposition techniques (SnO_2 [3–7], ZnO [3,8–10], In_2O_3 [3,11], Ga_2O_3 [12–14], SiO_2 [15–17], MgO [18,19], PbO_2 [20], etc. – see references for some detailed examples) in a quasi-1D form, where 'quasi' means that their smaller dimension is in the nano-scale range but it is generally too large to give rise to quantum confinement effects (e.g. the critical Bohr radius is reported to be 2.15–2.4 nm in In_2O_3 [11,21]). Nevertheless the 'reduced' dimension of these nanowires, together with the frequent natural non-stoichiometry of these oxides, gives rise to peculiar properties which are different from those of bulk material.

The number of successful reports in literature about the synthesis of In_2O_3 nanowires is much smaller than those for zinc oxide or tin oxide nanowires. This can testify that the growth of these nanostructures by a simple physical method is not trivial. The reason for such a difficulty may rise from the intrinsic high symmetry of the cubic crystal cell of In_2O_3.

To overcome this problem, metal catalysts, such as Au, Ag, or Ni [22–29], have been often used to force the In_2O_3 crystals to follow a highly oriented growth through a VLS (vapour–liquid–solid) mechanism. On the other hand, some authors [30,31] reported that In_2O_3 nanowires and branched nanostructures can also be obtained without catalysts by a carbothermal reaction with an In_2O_3 or In source.

Unfortunately the use of catalysts or other reagents (like carbon, nitrates, other reducing/oxidizing compounds, In precursors, etc.) may introduce undesired dopants inside the nanowires or leave alloys particles on the growth tip that may affect the nanowires properties.

Here we present the results of a simple process in which vapor transport, condensation and oxidation are employed, involving only metallic indium and oxygen in the reaction. Especially the role of the liquid indium phase is discussed. The optical constants are determined by Jasco 570 double beam spectrophotometer for optoelectronic applications and the results are compared with results obtained using other preparation methods, the PL properties of the In_2O_3 nanowires have been studied at room temperature.

2. Experimental

The preparation of In_2O_3 nanowires was carried out in a conventional horizontal tube furnace. The high purity (99.999%) of metal indium granulated was placed in an alumina boat as the source, and several wafer and *quartz* substrates were placed downstream along the tube, where a strong temperature gradient is expected. The furnace was then heated up to a maximum temperature of 1200 °C, while a small amount of inert gas (argon) flew along the tube. After two minutes oxygen was introduced into the reaction system by mixing it with the argon flow and 40 min later the furnace was cooled down to room temperature. The substrates, on which

* Corresponding author. Tel.: +20 1129264358; fax: +20 93 4601159.
E-mail address: nomery_abass@yahoo.com (N.M.A. Hadia).

0925-8388/$ - see front matter © 2012 Elsevier B.V. All rights reserved.
http://dx.doi.org/10.1016/j.jallcom.2012.08.116

In_2O_3 was deposited within a 500–1050 °C temperature range, were easily removed from the furnace and directly characterized by several techniques. The general structure was determined by by X-ray diffraction using a Schimadzu 7000 diffractometer. The diffraction patterns were obtained using Cu-Kα radiation (λ = 0.15406 nm), images obtained with a (JEOL JSM 6360LA, Japan) scanning electron microscope (SEM). The optical transmittance (T) of the In_2O_3 film was studied using a Jasco 570 double beam spectrophotometer in the wavelength (λ) range of 200–2500 nm at normal incidence. For further considerations, Photoluminescence (PL) measurements were performed using a 337 nm ILGI 503 N_2 laser.

3. Results and discussion

3.1. Structural and morphological of In_2O_3 nanostructures

The substrates were put along the furnace tube to collect samples with In_2O_3 crystals grown in different conditions. Indeed, the high temperature gradient in the growth/collection region generated a variety of local conditions, in which both vapor and liquid In phases may be present in various concentrations. This circumstance gave rise to different growth mechanisms that can be observed in the numerous collected In_2O_3 samples.

At high temperature (1050–900 °C) and high vapor pressure values the growth generally results in large In_2O_3 crystals (Fig. 1a). But in some special conditions, when the oxygen–argon ratio was not too high, some VLS match-like wires can grow (Fig. 1b). Differently from a common catalyzed VLS growth, in which the metal drop on the growth tip is made of Au or other metals that act as interface solutions, here the drop is made of In (see also [30,31]). Being In an active reagent in the In_2O_3 nanowire growth, it 'consumes' during the growth of the nanowire. So, this kind of growth was possible only when the vapor-to-liquid (vapor-to-drop) condensation rate is higher, or at least comparable, with the oxidation and growth rate, i.e. only at very high In vapor pressure values. At low temperature (<600 °C) In_2O_3 was present on the substrates in the shape of octahedral nanocrystals (Fig. 1c). These nanocrystals seem to generate directly in the vapour phase and then precipitate onto the substrates. Indeed they are not 'attached' to the substrate and they can be easily removed by any gentle blow.

Between these two temperature regions the used growth setup and conditions favor liquid In condensation during the first step of the growth (vapor transport). Inside this intermediate region, where the temperature is about 900 °C large metal droplets can be found even at the end of the growth, i.e. after the oxidation step. Condensation of In homogeneously decreases along the furnace and temperature gradient and, at about 600 °C, it is practically reduced to zero. Between 700 and 800 °C, where In condensation was not 'too strong' or 'too weak', a dense entanglement of In_2O_3 nanowires generally grows (Fig. 2a). Depending on the growth parameters, samples with different dimensions can be collected. The largest nanowires usually have a 'belt-like' or 'tape-like' rectangular section (Fig. 2b). Their thickness is in the 30–190 nm range, the width is about 5–10 times larger and they can be few hundreds of micrometers long. The smallest nanowires, instead, have a 10–30 nm round section.

Fig. 3 shows the XRD patterns of the obtained In_2O_3 nanowires. All the peaks in the XRD pattern could be indexed to cubic In_2O_3 with a lattice constant of a = 10.11 Å (JCPDS card No. 06-0416). Moreover, no other impurity phases were detected.

The size distribution was generally larger in the collected samples than in those reported in literature for VLS growths catalyzed with metals. TEM images revealed that there was no In metal particle at the end of the nanowires (on the growth tip) and so this means that, in the used growth process, the nanowire size could not be directly controlled by the size of metal droplets.

No In metal droplet is found on the growth tip, but in this growth the mechanism does not seem to be simply a 'direct VS (vapour–solid)' one, as those reported and discussed for other growths in literatures (e.g. see Refs. [30,31]). In this growth it has been observed, indeed, that In_2O_3 nanowires grow only in the region where some condensation of indium occurs. Hence the liquid phase is involved also in this growth, even if not in the usual vapor–liquid–solid mechanism reported in the literature. Studying the samples with a lower density of nanowires, it has been observed that the In_2O_3 nanowires generally grow starting from the edges of micron-size faceted In_2O_3 crystals (Fig. 4), while no nanowire has been found to elongate directly from the surface of the substrates. Even if the definition of the whole growth mechanism require further investigations, it is clear that liquid In condensation acts as a catalyst for the growth of In_2O_3 nanowires, in a 'self-catalytic' process. On the opposite, it has been observed that when the transport flow is slightly increased and In vapour does

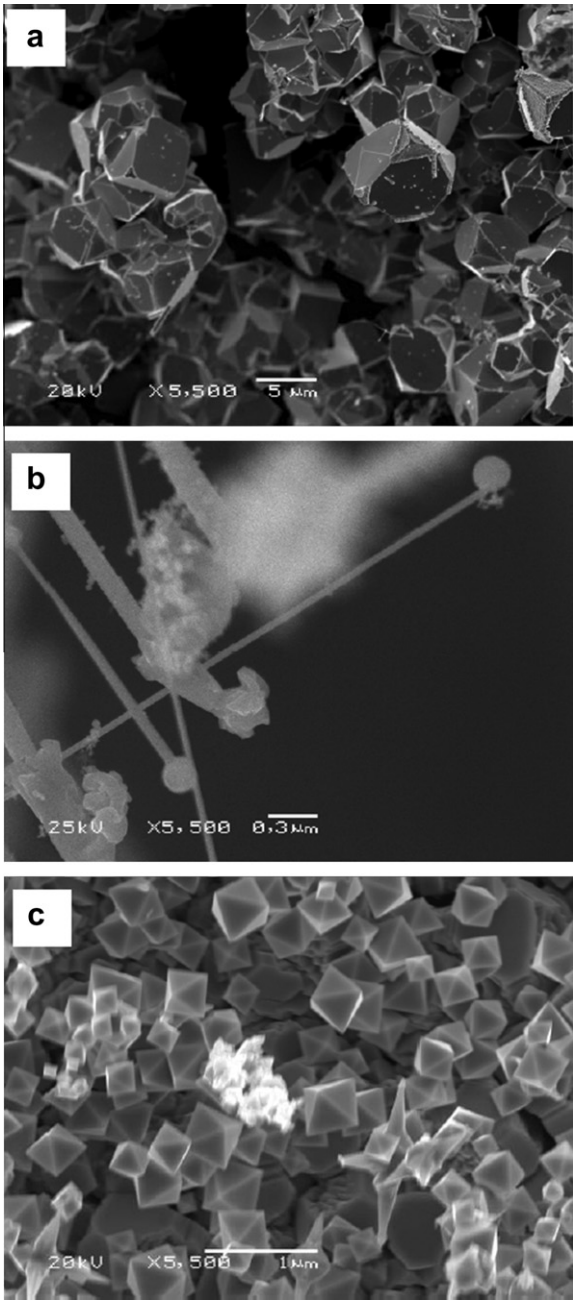

Fig. 1. SEM images of In_2O_3 crystals growth in different zones of the reactor: (a) large In_2O_3 crystals grown at high temperature; (b) In_2O_3 whiskers-like nanowires with a In metal drop at the top (also grown at high temperature); (c) In_2O_3 octahedral nanocrystals grown from the vapor phase and collected downstream at low temperature.

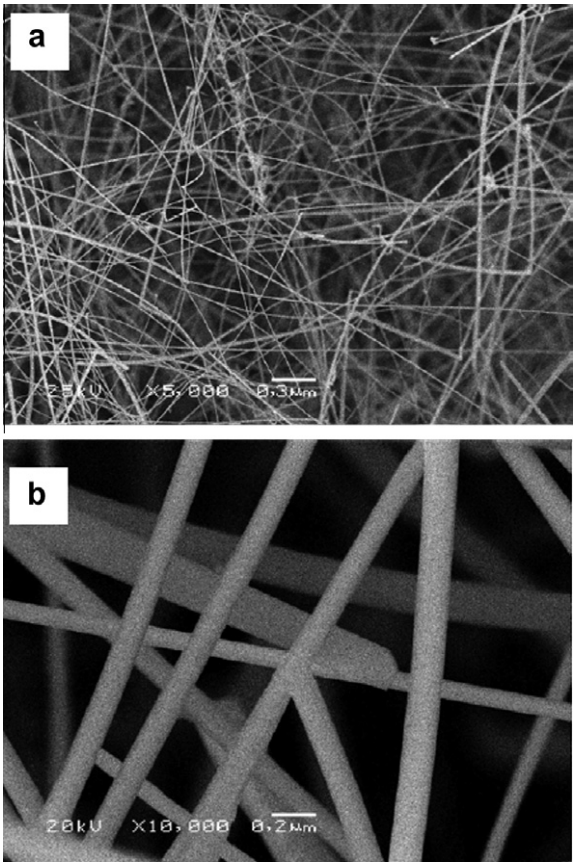

Fig. 2. SEM images of In_2O_3 nanowires: (a) a general view of the In_2O_3 nanowires deposition; (b) In_2O_3 nanorods with rectangular section.

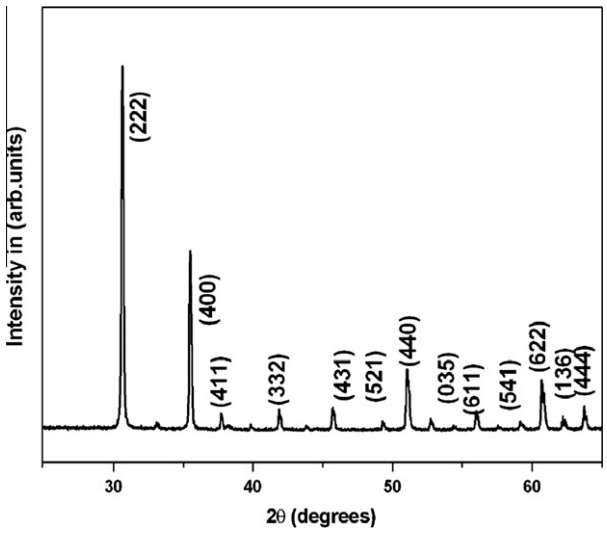

Fig. 3. XRD pattern of the synthesized In_2O_3 nanowires.

not condense in the usual growth region (In condensation is found only in the colder region of the reactor) nanowires cannot be obtained and only In_2O_3 octahedra are collected.

3.2. Optical properties of In_2O_3 nanowires

Fig. 5 shows the transmittance spectra of In_2O_3 NWs, measured in the wavelengths between 200 and 2500 nm. The optical transmission fell very sharply near the UV region due to the onset of

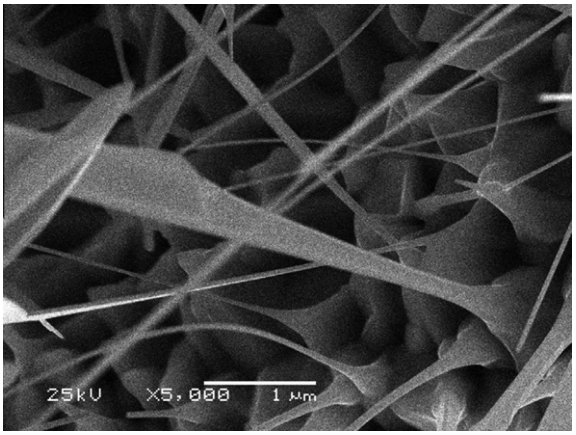

Fig. 4. In_2O_3 nanowires originate and grow starting from a In_2O_3 crystal edge.

fundamental absorption. The spectra showed a high transmittance, for the Samples. The higher transmittance observed in the samples was attributed to less scattering effects, structural homogeneity and better crystallinity, whereas, the lower transmittance might be due to the less crystallinity leading to more light scattering [32,38]. Furthermore, the fundamental absorption edge was shifted towards shorter wavelengths with the increase of deposition temperature, suggesting the widening of energy band-gap in the films due to Moss–Burstein shift as reported [33].

The absorption coefficient, α in the strong absorption region where the envelop method is not valid as the region was interference free, was evaluated from the optical transmittance data using Lambert's principle.

$$\alpha = (1/t)\ln T \tag{1}$$

where T is the transmittance and t is the thickness of the film. In the lower absorption region of the interference zone, the absorption coefficient could be calculated using the relation [34],

$$\alpha = -\frac{1}{t}\left\{\ln\left[\frac{E_M - [E_M^2 - (n^2-1)^3(n^2-s^4)]^{1/2}}{(n-1)^3(n-s^2)}\right]\right\} \tag{2}$$

where n is the refractive index of the film; s is the refractive index of substrate; T_M is the maximum transmission spectra and $E_M = (8n^2 s/T_M) + (n^2-1)(n^2-s^2)$.

The absorption coefficient was determined to be $\sim 2.3 \times 10^5$ cm^{-1} at the absorption edge.

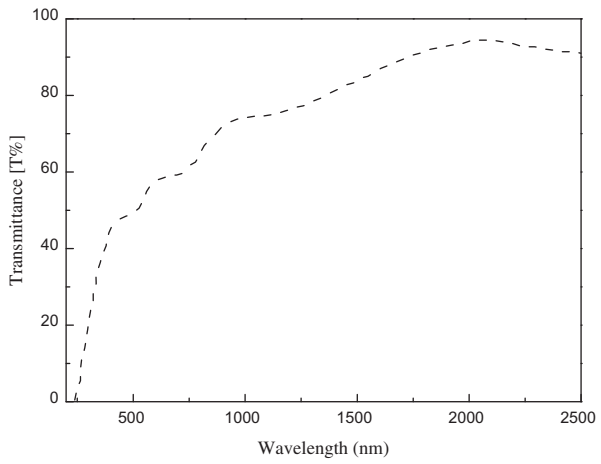

Fig. 5. Transmittance spectra of the synthesized In_2O_3 nanowires.

Fig. 6a shows the spectral dependence of absorption coefficient in In_2O_3 NWs. It could be observed that the absorption coefficient increased with the increase of photon energy and showed a tail in the low energy region ($h\nu < E_g$). This indicated that there was a high concentration of impurity states causing the band structures to perturb, resulting in a prolonged tail extending into the energy gap in polycrystalline films [35]. An exponential increase in the absorption edge followed the Urbach empirical equation [14],

$$\alpha = \alpha_0 \exp\left[\frac{h\nu - E_1}{E_0}\right] \quad (3)$$

where E_0 and α_0 are characteristic parameters of the material, represented as the Urbach energy width of the exponential tail and Urbach absorption energy. According to the Eq. (3), the plot of ln α as a function of photon energy, E gives a straight line. The extrapolation of these lines converges at a point E_1 called as 'focal point'. The Urbach tails were observed for the sample. The values of α_0 and E_0 were $2.69 \times 10^4\ cm^{-1}$ and ≈576 meV, respectively and the focal point was at $E_1 \approx 4.24$ eV. Melsheimer and Ziegler [36] interpreted the width, E_0 as a function of structural disorder, which decreases with the increase of structural order. This behavior of E_0 is in good agreement with our present observation for the sample.

The type of optical transition and the energy band gap of In_2O_3 NWs could be determined from the dependence of absorption coefficient, α on the photon energy, $h\nu$. The direct or indirect nature of optical transition between parabolic bands could be studied using the relation [37],

$$(\alpha h\nu) = A(h\nu - E_g)^x \quad (4)$$

where A is a constant, E_g is the optical energy band gap, $x = 1/2$ and 3/2 for the direct allowed and direct forbidden transitions, respectively. Furthermore, the value of $x = 2$ and 3 for the indirect allowed and indirect forbidden transitions, respectively. In the present study, the variation of absorption coefficient with photon energy followed the above relation for $x = 1/2$ indicating that the transition must correspond to a directly allowed electronic transition. Fig. 6b shows a plot of $(\alpha h\nu)^2$ versus $h\nu$ and the variation of energy band gap in the In_2O_3 NWs is shown in the inset. The energy band gap was determined by extrapolation of the linear portion of $(\alpha h\nu)^2$ versus $h\nu$ plot onto the energy axis and was found to be 3.33 ± 0.02 eV. Joseph Prince et al. reported a similar variation of band gap with growth temperature in spray deposited In_2O_3 thin films and attributed to Burstein–Moss shift where the increase in the optical band gap was related to an increase in the electron concentration leading to the rise of Fermi level within the conduction band in degenerate semiconductors [33,38].

Fig. 7a shows the variation of refractive index with wavelength where the solid curve represents the Cauchy fit. The refractive index n of the film was found to decrease continuously with the increase of wavelength following the Kronig–Krammer's relation. The value of refractive index was evaluated as 1.92 at 500 nm, which is lower than the reported value of 2.0 [39]. This might be due to the lower packing density of grains in the films. The refractive index is an important tool to detect the packing density.

The extinction coefficient (k) was directly calculated from the absorption coefficient by using the relation [40],

$$k = \frac{\alpha\lambda}{4\pi} \quad (5)$$

The evaluated value of extinction coefficient had a maximum at the absorption edge. The variation of extinction coefficient with wavelength is shown in Fig. 7b. It indicated a sharp fall in the value

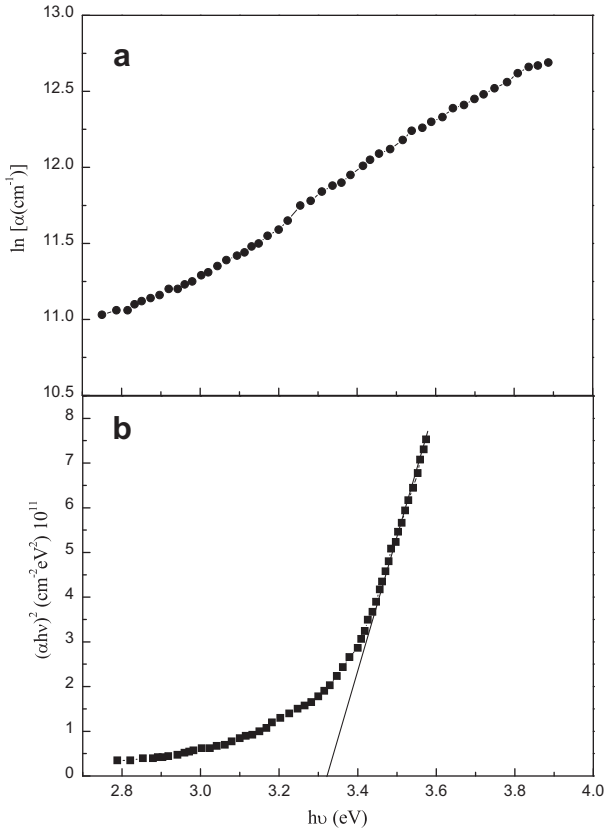

Fig. 6. Variation of absorption coefficient as a function of photon energy (a) and $(\alpha h\nu)^2$ versus $h\nu$ plot of In_2O_3 nanowires (b).

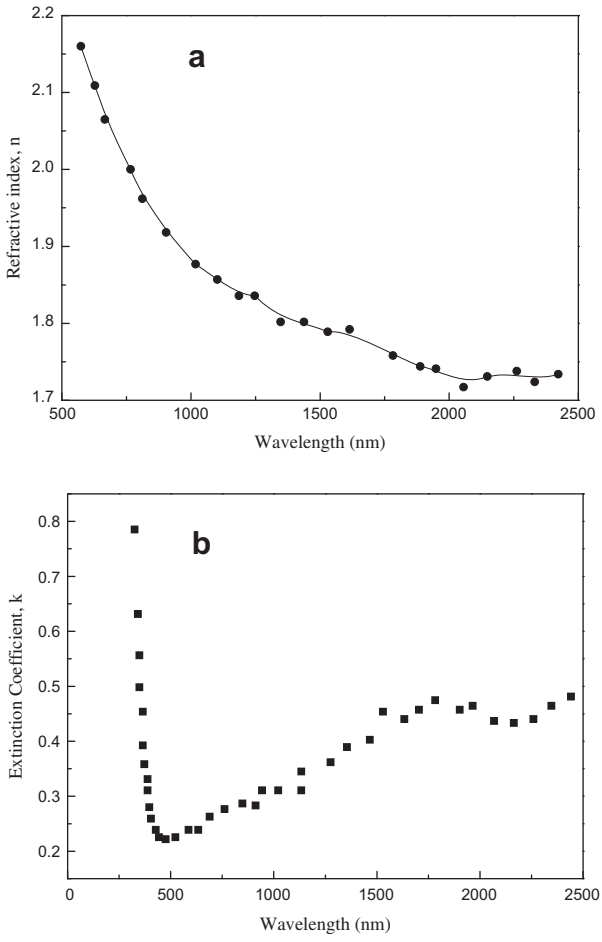

Fig. 7. The refractive index (a) and extinction coefficient (b) of In_2O_3 nanowires.

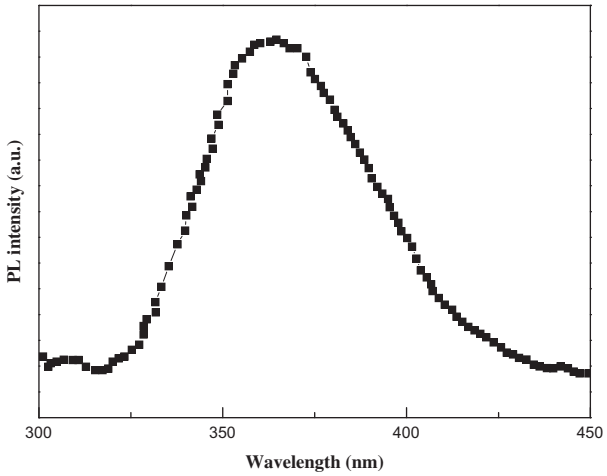

Fig. 8. PL spectrum of the In_2O_3 nanowires at room temperature.

of k at lower wavelengths and reached a minimum at a wavelength close to the energy band gap for the film. The change of k above this value of wavelength was marginal. The value of extinction coefficient was found to be high for the film that may be due to the crystallographic defects such as grain boundaries and voids present in the layers. This may be due to an improvement in the crystallinity leading to minimum imperfections. In the near infrared region, the origin of high extinction coefficient may be due to the interaction of light with the free carriers as the plasma wavelength for the present film.

3.3. Photoluminescence (PL) In_2O_3 nanowires

Fig. 8 shows room temperature PL spectrum of In_2O_3 nanowires sample. A broad and intense UV emission centering at ~375 nm was obtained [40]. In_2O_3 nanowires are known as n-type semiconductor with oxygen vacancies acting as the donors [41]. Thus the UV emission may originate from the transition of the oxygen donor level to the valence band. It is known that a large amount of oxygen deficiencies is generally associated with single crystalline In2O3, due to the partial or incomplete oxidation of metallic In particles during the rapid evaporation process [42].

4. Conclusions

In_2O_3 nanowires have been grown directly from metal indium and oxygen to obtain high-purity crystals without catalysts. In this study, liquid In can play the role of 'self-catalyst' and it easily allows to get In_2O_3 nanowires. Using this process, good quality single nanocrystals can be collected directly onto the substrates. The impurity level in these In_2O_3 nanowires is expected to be lower than in those of catalyzed VLS growths. In_2O_3 films were deposited by chemical spray pyrolysis. The optical properties of the In_2O_3 nanowires were determined by using optical transmittance data. The film had an absorption coefficient, $\alpha \sim 10^5\ cm^{-1}$. The optical band gap of the film was 3.33 eV. The refractive index was found to decrease continuously with the increase of wavelength. The value of n varied in the range ~1.8–2.22 and followed the Cauchy relation indicating that normal dispersion was present in the samples. The spectral dependence of extinction coefficient also showed its variation from ~0.2 to 0.8.

Acknowledgments

The authors extend their appreciation to the Research Center of Teachers College, King Saud University for funding this work through the research group Project No RSP-TCR-05.

We would like to thank Prof. Dr. S.V. Ryabtsev (Department of Solid State Physics and Nanostructure, Faculty of Physics, Voronezh State University, Voronezh, Russia.) for helping us.

References

[1] I.M. Tiginyanu, O. Lupan, V.V. Ursaki, L. Chow, M. Enachi, Compr. Semiconductor Sci. Technol. 3 (2011) 396.
[2] A. Vomiero, I. Concina, E. Comini, C. Soldano, M. Ferroni, G. Faglia, G. Sberveglieri, Nano Energy 1 (2012) 372.
[3] J.H. Shin, J.Y. Song, Y.H. Kim, S.D. Kim, H.M. Park, Mater. Lett. 66 (2012) 106.
[4] J. pan, H. Shen, S. Mathur, J. Nanotechnol. 2012 (2012). ID 917320 12.
[5] S.H. Mohamed, J. Alloys Comp. 510 (2012) 119.
[6] L. Zanotti, M. Zha, D. Calestani, E. Comini, G. Sberveglieri, Cryst. Res. Technol. 40 (2005) 932.
[7] N.M.A. Hadia, S.V. Ryabtsev, E.P. Domashevskaya, P.V. Seredin, Eur. Phys. J. Appl. Phys. 48 (2009) 10603.
[8] P. Chandrasekaran, G. Viruthagiri, N. Srinivasan, J. Alloys Comp. 540 (2012) 89.
[9] J. Karamdel, C.F. Dee, G.K.G. Saw, B. Varghese, C.H. Sow, I. Ahmad, B.Y. Majlis, J. Alloys Comp. 512 (2012) 68.
[10] N.M.A. Hadia, H.A. Mohamed, J. Adv. Microsc. Res. 7 (2012) 32.
[11] Y. Huang, K. Yu, Z. Xu, Z. Zhu, Physica E 43 (2011) 1502.
[12] Z. Sun, L. Yang, X. Shen, Z. Chen, Chin. Sci. Bull. 57 (2012) 565.
[13] E.I. EL-Sayed, A.A. Al-Ghamdi, S. Al-Heniti, F. Al-Marzouki, F. El-Tantawy, Mater. Lett. 65 (2011) 317.
[14] S. Park, H. Kim, C. Jin, C. Lee, J. Korean Phys. Soc. 60 (2012) 1560.
[15] M. Ghahari, R. Aghababazadeh, T. Ebadzadeh, A. Mirhabibi, R. Brydson, P. Fabbri, F. Najafi, J. Nanosci. Nanotechnol. 6 (2011) 5311.
[16] A. Sadrmomtazi, A. Fasihi, Nanotechnol. Nanosci. 2 (2011) 42.
[17] Y. Yang, A. Shalav, T. Kim, R.G. Elliman, Appl. Phys. A 107 (2012) 885.
[18] C. Jin, H. Kim, S. Park, C. Lee, J. Alloys Comp. 541 (2012) 163.
[19] H.W. Kim, H.G. Na, J.C. Yang, D.S. Kwak, Thin Solid Films 520 (2012) 2627.
[20] D.P. Singh, O.N. Srivastava, Nano-Micro Lett. 3 (2011) 223.
[21] A. Qurashi, E.M. El-Maghraby, T. Yamazaki, Y. Shen, T. Kikuta, J. Alloys Comp. 481 (2009) 135.
[22] G. Chen, L. Wang, X. Sheng, H. Liu, X. Pi, Y. Zhang, D. Li, D. Yang, Nanoscale Res. Lett. 5 (2011) 898.
[23] H.S. Kim, H.G. Na, J.C. Yang, C. Lee, H.W. Kim, Acta Physica Polonica A 119 (2011) 143.
[24] T. Gao, T. Wang, J. Cryst. Growth 290 (2006) 660.
[25] S.Q. Li, Y.X. Liang, C. Wang, X.Q. Fu, T.H. Wang, Appl. Phys. Lett. 88 (2006) 163111.
[26] Y.X. Liang, S.Q. Li, L. Nie, Y.G. Wang, T.H. Wang, Appl. Phys. Lett. 88 (2006) 193119.
[27] W. He-Lin, Z. Lei, L. Zu-Li, Y. Kai-Lun, Chin. Phys. B 20 (2011) 118102.
[28] P. Papageorgiou, M. Zervos, A. Othonos, Nanoscale Res. Lett. 6 (2011) 311.
[29] J.S. Jeong, J.Y. Lee, Nanotechnology 21 (2010) 405601.
[30] K.C. Kam, F.L. Deepak, A.K. Cheetham, C.N.R. Rao, Chem. Phys. Lett. 397 (2004) 329.
[31] D. Calestani, M. Zha, A. Zappettini, L. Lazzarini, L. Zanotti, Chem. Phys. Lett. 445 (2007) 251.
[32] P. Thilakan, J. Kumar, Mater. Sci. Eng. B 55 (1998) 195.
[33] P. Prathap, Y.P.V. Subbaiah, M. Devika, K.T. Ramakrishna Reddy, Mater. Chem. Phys. 100 (2006) 375.
[34] R. Swanepoel, Phys. E: Sci. Instrum. 16 (1983) 1214.
[35] R.H. Parmenter, Phys. Rev. 97 (1955) 587.
[36] J. Melsheimer, D. Ziegler, Thin Solid Films 129 (1985) 35.
[37] A.L. Fahrenbruch, R.H. Bube (Eds.), Fundamentals of Solar Cells, Academic, New York, 1993.
[38] J.J. Prince, S. Ramamurthy, B. Subramanian, C. Sanjeeviraja, M. Jayachandran, J. Cryst. Growth 240 (2002) 142.
[39] W.W. Mobzen, J. Vac. Sci. Technol. 12 (1975) 99.
[40] A. Qurashi, E.M. El-Maghraby, T. Yamazaki, T. Kikuta, Sens. Actuators B 147 (2010) 48.
[41] F. Zeng, X. Zhang, J. Wang, L. Wang, L. Zhang, Nanotechnology 15 (2004) 596.
[42] P. Guha, S. Kar, S. Chaudhuri, Appl. Phys. Lett. 85 (2004) 3851.